A&A 473, 445–455 (2007)
DOI: 10.1051/0004-6361:20077675

Astronomy & Astrophysics

Old open clusters in the inner Galaxy: FSR 1744, FSR 89 and FSR 31

C. Bonatto and E. Bica

Universidade Federal do Rio Grande do Sul, Departamento de Astronomia, CP 15051, RS, Porto Alegre 91501-970, Brazil
e-mail: [charles;bica]@if.ufrgs.br

Received 19 April 2007 / Accepted 9 July 2007

ABSTRACT

Context. We examine the dynamical survival of intermediate-age/old open clusters in the inner Galaxy.
Aims. We aim to establish the nature and derive fundamental and structural parameters of the recently catalogued objects FSR 1744, FSR 89 and FSR 31 to constrain the Galactic tidal disruption efficiency, improve statistics of the open cluster parameter space, and better define their age-distribution function inside the Solar circle. The current status of the issue dealing with the small number of detected open clusters in the inner Galaxy is discussed.
Methods. Properties of the objects are investigated with 2MASS colour–magnitude diagrams and stellar radial density profiles built with field star decontaminated photometry. Diagnostic diagrams of structural parameters are used to separate dynamical from high-background effects affecting such centrally projected open clusters.
Results. FSR 1744, FSR 89 and FSR 31 are Gyr-class open clusters located at Galactocentric distances 4.0–5.6 kpc. Compared to nearby open clusters, they have small core and limiting radii.
Conclusions. With respect to the small number of open clusters observed in the inner Galaxy, the emerging scenario in the near-infrared favours disruption driven by dynamical evolution rather than observational limitations associated with absorption and/or high background levels. Internally, the main processes associated with the dynamical evolution are mass loss by stellar evolution, mass segregation and evaporation. Externally they are tidal stress from the disk and bulge, and interactions with giant molecular clouds. FSR 1744, FSR 89 and FSR 31 have structural parameters consistent with their Galactocentric distances, in the sense that tidally induced effects may have accelerated the dynamical evolution.

Key words. Galaxy: open clusters and associations: individual: FSR 1744 – open clusters and associations: individual: FSR 89 – open clusters and associations: individual: FSR 31 – Galaxy: structure

1. Introduction

Star clusters evolve dynamically because of internal (e.g. mass loss during stellar evolution, mass segregation and evaporation) and external (e.g. tidal interactions with the disk and Galactic bulge, and collisions with giant molecular clouds – GMCs) processes. As clusters age, their structure suffer significant changes, to the point that most end up completely dissolved in the Galactic stellar field or as poorly-populated remnants.

Probably reflecting the Galactocentric distance-dependent strength of the external tidal stress, there is an asymmetry in the age distribution of open clusters (OCs) in the Galaxy: old (age >1 Gyr) OCs are scarce and tend to be more concentrated towards the Galactic anti-center than young ones (e.g. van den Bergh & McClure 1980; Friel 1995; Bonatto et al. 2006a).

Historically, disruption was the primary effect assumed to explain the scarcity of OCs older than $\sim 10^8$–10^9 yr in the Galaxy, a fact that was almost simultaneously noted by van den Bergh (1957), Oort (1958) and von Hoerner (1958). On theoretical grounds, Spitzer (1958) calculated disruption time-scales ($t_{\rm dis}$) consistent with the old-age cutoff and indicated that collisions with interstellar clouds should also contribute to cluster disruption. Disruptive effects due to GMCs were investigated by Wielen (1971) and Wielen (1991), who estimated $t_{\rm dis} \sim 200$ Myr for 50% of the Milky Way OCs, and suggested a dependence of $t_{\rm dis}$ on cluster size and mass. Gieles et al. (2006) found $t_{\rm dis} \sim 2$ Gyr for the disruption of a $10^4\,M_\odot$ cluster due to encounters with GMCs, and suggested that the combined effect of tidal field and encounters with GMCs can explain the lack of old OCs in the solar neighbourhood. Further observational evidence for the dependence of the disruption time-scale on mass are given by Janes & Adler (1982) and Lamers et al. (2005, and references therein). The latter authors found $t_{\rm dis} \sim M^{0.62}$, which for cluster mass in the range 10^2–$10^3\,M_\odot$ corresponds to $75 \lesssim t_{\rm dis}({\rm Myr}) \lesssim 300$.

Indeed, the well-studied clusters in the central Galaxy are as a rule young and massive, and have not yet significantly responded to tidal effects. The Arches cluster, near the Galactic nucleus, has an age of 2 Myr and a mass $M = 10^5\,M_\odot$ (Figer et al. 2002), while the Quintuplet cluster is 4 Myr old and has an estimated mass $M = 1.3 \times 10^4\,M_\odot$ (Figer et al. 1999). BD 11 is not as massive as the Arches cluster, but is similarly young and close to the center (Dutra et al. 2003a).

The disk ring $1 < R_{\rm GC}({\rm kpc}) < 3$ contains the noteworthy clusters Westerlund 1 and BDSB 122. Westerlund 1 is located at $d_\odot \approx 5$ kpc with an age of 4.5–5 Myr (Crowther et al. 2006). Its initial mass is estimated to be $M \approx 10^5\,M_\odot$ (Clark et al. 2005). Bica et al. (2003a) discovered the cluster BDSB 122 and Figer et al. (2006) estimated it to be very massive with $M \approx 2$–$4 \times 10^4\,M_\odot$. BDSB 122 contains 14 red supergiants with an age of 7–12 Myr at $d_\odot = 5.8$ kpc.

Despite the above observational and theoretical efforts, old OCs within $\lesssim$4 kpc of the Galactic centre remain virtually

undetected (e.g. Bonatto et al. 2006a). Although conceptually different processes, tidal shocks (from the Galaxy and GMCs) and observational completeness may combine to explain the scarcity of central clusters. Absorption and crowding in fields dominated by the disk and bulge stars are expected to significantly decrease completeness, especially at the faint-end of the OC luminosity distribution. Indeed, using a sample of 654 OCs with available fundamental parameters, Bonatto et al. (2006a) found that a large fraction of the intrinsically faint and/or distant OCs must be drowned in the field contamination, particularly in bulge/disk directions.

Undoubtedly, the nuclear clusters face dissolution (Portegies Zwart et al. 2002). Based on arguments related to observational completeness affecting the spatial distribution of the Galactic OCs, Bonatto et al. (2006a) found that tidal disruption may begin to be important for OCs located at distances $\gtrsim$1.4 kpc inside the Solar circle. A fundamental question is whether massive clusters in the intermediate ring $1 < R_{\rm GC}({\rm kpc}) < 3$, such as Westerlund 1 and BDSB 122, might survive to old ages.

Froebrich et al. (2007b) have presented a catalogue of 1021 cluster candidates (hereafter FSR objects) at Galactic latitudes $|b| < 20^\circ$ and all longitudes, by means of an automated algorithm applied to the 2MASS[1] database. In the present study we search for old OC candidates towards the central parts of the Galaxy from the targets in that catalogue. Detection of such objects will help constrain the dynamical survival issue.

Recent determinations of the distance of the Sun to the Galactic center by different methods show decreasing values as compared to the usual $R_\odot = 8.0$ kpc (Reid 1993). Eisenhauer et al. (2005) found $R_\odot = 7.6 \pm 0.3$ kpc, Nishiyama et al. (2006) obtained $R_\odot = 7.5 \pm 0.35$ kpc, and Bica et al. (2006) $R_\odot = 7.2 \pm 0.3$ kpc. The latter value, based on updated distances of globular clusters, is adopted throughout the present paper.

In the present work we investigate the nature of three candidates to old OCs in the inner Galaxy by means of near-infrared colour-magnitude diagrams (CMDs) and cluster structural parameters. In Sect. 2 we discuss aspects related to the dynamical evolution and disruption of star clusters. In Sect. 3 we discuss the spatial distribution of the known old OCs. In Sect. 4 we analyse CMDs and compute cluster fundamental parameters. In Sect. 5 we derive structural parameters. Discussions on the nature of the objects are provided in Sect. 6. Concluding remarks are given in Sect. 7.

2. Considerations on dynamical evolution and disruption

Star clusters form in collapsing molecular clouds in which variable fractions (10–30%, e.g. Lada & Lada 2003) of the parent gas are converted into stars. They remain embedded in the clouds for about 2–5 Myr, and their dynamical state at that early phase can be described as out of virial equilibrium (e.g. de la Fuente Marcos & de la Fuente Marcos 2002). Following the rapid expulsion of the unused gas by massive winds and supernovae, stars end up with exceeding velocities with respect to the new, decreased, potential (e.g. de la Fuente Marcos & de la Fuente Marcos 2002; Boily & Kroupa 2002; Goodwin & Bastian 2006). As a consequence, clusters expand on all scales as they progress towards virialization. Reflecting the violent structural changes associated with this early phase, the number of optically detected clusters, i.e. those that survived the infant mortality, is significantly smaller than the number of embedded clusters ($\approx$4%, Lada & Lada 2003).

N-body simulations of massive star clusters that include the effect of gas removal (e.g. Goodwin & Bastian 2006) consistently show that the phase of dramatic core radius increase may last about 10–30 Myr. They also suggest that after a few 10^7 yr, core growth levels off as some energy equipartition is reached. The outer parts, on the other hand, keep expanding and become loosely bound. Theoretically, the subsequent core evolution depends on several factors such as cluster mass and the relative efficiencies of energy equipartition, evaporation and gravothermal instability. These processes tend to produce a phase of core contraction that may be followed by a rapid expansion, which is confirmed by *N*-body simulations of clusters with less than 20 000 particles and stars with two different masses (e.g. Khalisi et al. 2007). An alternative effect that also leads to core contraction, at least in the early phases, is the violent relaxation that follows from the time-dependent potential resulting from rapid gas removal (Bastian & Goodwin 2006; Kroupa et al. 2001). Thus, mass loss (from gas removal or stellar evolution) leads to cluster expansion on all scales at the early phases, while dynamical friction in a multi-mass system leads to core collapse/contraction at later phases.

With respect to other galaxies, most LMC and SMC clusters follow a trend of increasing core radius with cluster age, but there is observational evidence for clusters in a phase of core shrinkage occurring at several hundred Myr (e.g. Mackey & Gilmore 2003). Considering the very different time-scales involved, early gas removal (Goodwin & Bastian 2006) cannot explain the core shrinkage at such later phases.

Observational evidence of a dependence of the core mass function slope (and radius) on the dynamical-evolution parameter $\tau = {\rm Age}/t_{\rm rel}$, where $t_{\rm rel}$ is the relaxation time, was found for a set of nearby OCs by Bonatto & Bica (2005, 2007). The dependence occurs in the sense that dynamically old clusters tend to have shallow core mass functions and, for some of the clusters, small core radius. Similar relations were found in a sample of 42 OCs by BV CCD photometry (Maciejewski & Niedzielski 2007), and in 9 others with wide-field CCD photometry (Sharma et al. 2006).

Eventually, most clusters are destroyed by internal processes (mass loss caused by the dynamical and stellar evolution) or leave remnants (Pavani & Bica 2007, and references therein). On the other hand, higher efficiencies of star formation ($\gtrsim$30%) are predicted to enhance cluster survival rates. Such clusters can reach old ages, although the final clusters retain only a small fraction of the initial mass (Goodwin & Bastian 2006).

At the same time, interactions with the disk, the tidal pull of the Galactic bulge, and collisions with GMCs (Sect. 1) tend to destroy the poorly-populated OCs on a time-scale of a few 10^8 Myr (Bergond et al. 2001), especially in the inner Galaxy. Indeed, van den Bergh & McClure (1980) noted that OCs older than $\gtrsim$1 Gyr tended to be concentrated towards the anti-center, a region with a low density of GMCs. The observation that the fraction of old clusters in the LMC and SMC is higher than in the Galaxy suggests that the disruption time-scale may not be the same in all galaxies (Elson & Fall 1985; Wielen 1985; Hodge 1987), instead, it may vary with the different GMC densities in those galaxies.

Over long time periods, the net effect of tidal interactions on a star cluster is to heat it, in the sense that its stars gain more kinetic energy after each event, which leads to an increase in the evaporation rate. Recent works estimate that the central

[1] The Two Micron All Sky Survey, available at www.ipac.caltech.edu/2mass/releases/allsky/

($R_{GC} \lesssim 150$ pc) tidal fields can dissolve a massive star cluster in ≈50 Myr (Portegies Zwart et al. 2002). Near the Solar circle most OCs appear to dissolve on a time-scale shorter than ∼1 Gyr (Bergond et al. 2001; Bonatto et al. 2006a), consistent with the 1.3±0.5 Gyr estimate for a $10^4\,M_\odot$ cluster found by Lamers et al. (2005). These time-scales are intermediate between those predicted from N-body simulations of OCs in the tidal field of the Solar vicinity (∼6.3 Gyr, Baumgardt & Makino 2003) and the 322 ± 31 Myr derived for Piskunov et al. (2007a). Differences between these time-scales probably reflect a dependence of disruption on cluster mass, since the relatively short time-scales of Piskunov et al. (2007a), Bonatto et al. (2006a) and Bergond et al. (2001) correspond to OCs of lower mass ($\lesssim 10^3\,M_\odot$) than the $10^4\,M_\odot$ used in the models of Lamers et al. (2005). The large time-scale of Baumgardt & Makino (2003) probably results because their models do not include external perturbations.

Except for the N-body time-scale, the remaining ones are consistent with the fact that old OCs (age $\gtrsim$ 1 Gyr) are usually found near the Solar circle and in the outer Galaxy (e.g. Friel 1995; Bonatto et al. 2006a), where the frequency of potentially damaging dynamical interactions with GMCs and the disk is low (e.g. Salaris et al. 2004; Upgren et al. 1972). In addition, simulations show that the initial mass function, fraction of binaries, total mass and Galactocentric distance are factors intimately linked to cluster lifetimes (e.g. Terlevich 1987; de La Fuente Marcos 1997; de La Fuente Marcos 1998). Considering these aspects, the dynamical survival rate of star clusters, especially in the inner Galaxy, can possibly be used to probe the tidal field of the Galaxy.

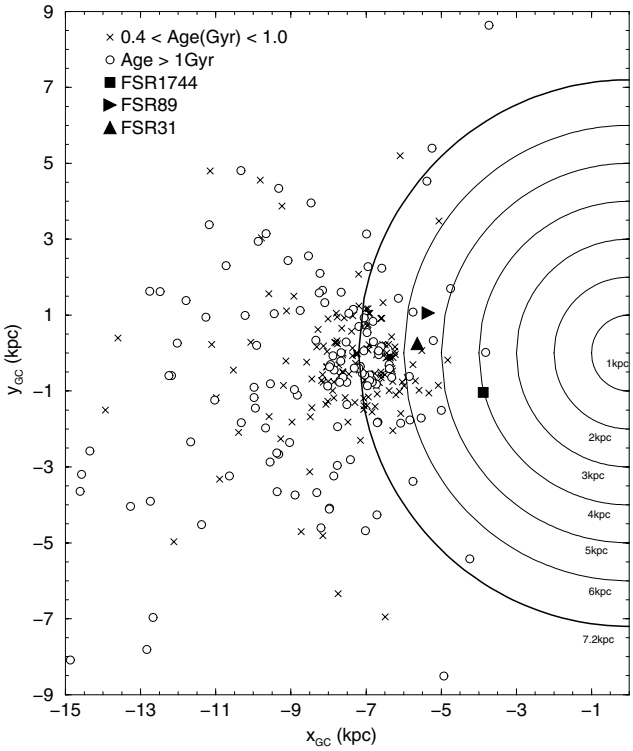

Fig. 1. Spatial distribution of the WEBDA OCs with ages 0.4–1 Gyr (crosses) and older than 1 Gyr (empty circles). The semi-circles indicate Galactocentric distances from 1 to 7.2 kpc. The position of the candidates to old OCs FSR 1744, FSR 89 and FSR 31 are shown (Sect. 4).

3. An overview of the evolved and old open clusters

The WEBDA[2] database (Mermilliod 1996) provides updated parameters for the studied optical OCs. We selected from WEBDA the OCs with age in the range 0.4–1 Gyr, and those older than 1 Gyr, for which we compute the projections on the Galactic plane of the Galactic coordinates (ℓ, b) $x_{GC} = d_\odot \cos(b)\cos(\ell) - R_\odot$ and $y_{GC} = d_\odot \cos(b)\sin(\ell)$, where $d_\odot$ is the distance from the Sun and $R_\odot = 7.2$ kpc (Bica et al. 2006). The x_{GC} and y_{GC} distributions are shown in Fig. 1. Both age groups share a similar spatial distribution, in which the number-density of OCs decreases with Galactocentric distance beyond the Solar circle (e.g. Friel 1995; Bonatto et al. 2006a).

A systematic inspection of the 2MASS images of the FSR candidates carried out by one of us (EB) revealed that in the Galactic longitude zone $|l| < 30°$, the 3 objects FSR 1744, FSR 89 and FSR 31, appear as probable OCs. Another interesting object in that zone is FSR 1735, probably a globular cluster (Froebrich et al. 2007a).

Figure 1 shows the positions of FSR 1744, FSR 89 and FSR 31, based on the Galactocentric distances and components computed in Sect. 4. They are located at $4 \lesssim R_{GC}(\mathrm{kpc}) \lesssim 6$, with FSR 1744 being the innermost at $R_{GC} = 4.0$ kpc (Sect. 4).

In Fig. 2 we further explore the spatial properties of FSR 1744, FSR 89 and FSR 31 with respect to those of the OCs older than 0.4 Gyr. The relation of the distance to the Galactic plane ($|Z|$) with Galactocentric distance is shown in panel (a). Only old OCs are found at $R_{GC} \gtrsim 14$ kpc and $|Z| \gtrsim 0.65$ kpc, as previously noted by e.g. van den Bergh & McClure (1980). This should be expected, since OCs in the outer disk and/or in regions high above the plane spend most of their orbits far away from the disruptive effects associated with the central Galactic regions and GMCs (e.g. Friel 1995). Panels (b) and (c) contain histograms for the number of OCs (in each age range) as a function of Galactocentric distance and distance to the Galactic plane, respectively. They 3 old OCs located among the innermost ones in the Galaxy. As already suggested by their low Galactic latitudes (Table 1) they are within ≈100 pc of the plane. Consequently, they are expected to be affected by important field-star contamination.

4. Photometric parameters with 2MASS

The original coordinates of FSR 1744 (Froebrich et al. 2007b) are slightly shifted with respect to the central concentration of stars as seen in 2MASS images (e.g. Fig. 3). The revised values, together with the original ones for the three objects, are given in Table 1. Table 1 also provides the following parameters derived in the present work, by columns, cluster age (9), reddening $E(B-V)$ (10), distance from the Sun (11), and Galactocentric distance (12), derived in the subsequent analyses.

2MASS H images covering a $4' \times 4'$ field of the target objects are shown in Figs. 3–5. In all cases a concentration of stars is superimposed on crowded fields, as expected from such central directions, especially for FSR 31 (Table 1).

4.1. 2MASS photometry

J, H and K_s 2MASS photometry was extracted in circular fields centred on the optimized coordinates of the objects (Cols. 5 and 6 of Table 1) using VizieR[3]. Our previous experience with

[2] obswww.unige.ch/webda

[3] vizier.u-strasbg.fr/viz-bin/VizieR?-source=II/246

Table 1. Fundamental parameters.

Cluster	FSR2007			Present results derived from 2MASS data							
	α(2000)	δ(2000)	D	α(2000)	δ(2000)	ℓ	b	Age	$E(B-V)$	$d_\odot$	R_{GC}
	(hms)	(°′″)	(′)	(hms)	(°′″)	(°)	(°)	(Gyr)		(kpc)	(kpc)
(1)	(2)	(3)	(4)	(5)	(6)	(7)	(8)	(9)	(10)	(11)	(12)
FSR 1744	16:51:36	−42:24:55	2.2	16:51:32	−42:25:57	342.68	+1.18	1.0 ± 0.1	2.56 ± 0.12	3.5 ± 0.1	4.0 ± 0.1
FSR 89	18:48:39	−03:30:34	2	18:48:39	−03:30:34	29.49	−0.98	1.0 ± 0.1	2.94 ± 0.10	2.2 ± 0.1	5.4 ± 0.1
FSR 31	18:06:29	−21:22:33	6	18:06:29	−21:22:33	8.91	−0.27	1.1 ± 0.2	1.47 ± 0.09	1.6 ± 0.1	5.6 ± 0.1

Notes. Columns 2 and 3: central coordinates provided by Froebrich et al. (2007b); Col. 4: angular diameter estimated on the 2MASS images (Figs. 3–5); Cols. 5–8: optimized central coordinates (from 2MASS data); Col. 10: reddening in the object's central region (Sect. 4); Col. 12: R_{GC} calculated using $R_\odot$ = 7.2 kpc (Bica et al. 2006) as the distance of the Sun to the Galactic centre.

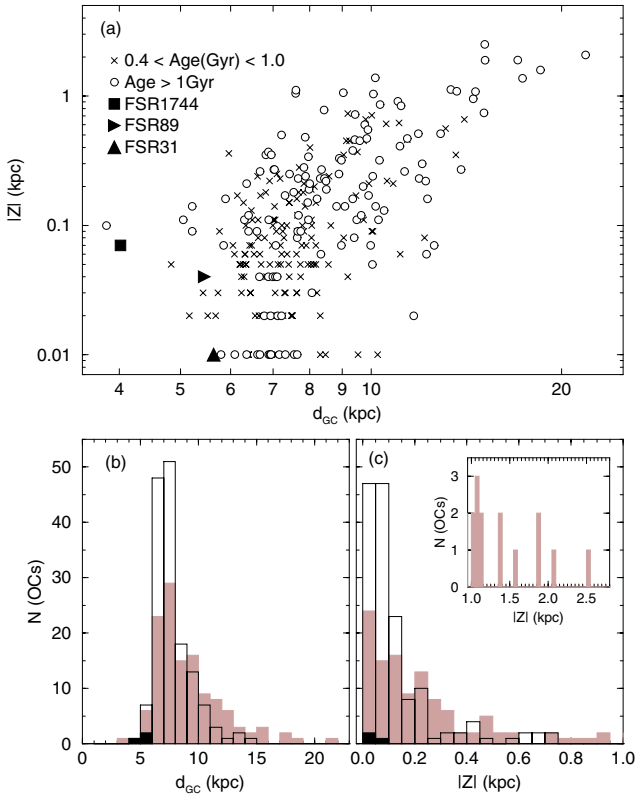

Fig. 2. Panel **a)**: relation of distance from the plane $|Z|$ with R_{GC} for the OCs older than 1 Gyr (empty circles) and those with age in the range 0.4–1.0 Gyr (crosses). The respective R_{GC} and $|Z|$ histograms are shown in panels **b)** and **c)** for OCs older than 1 Gyr (gray histograms), those with ages 0.4–1.0 Gyr (empty), and the present objects (black). The inset in panel **c)** contains the OCs at $|Z| > 1.0$ kpc. These are all older than 1 Gyr.

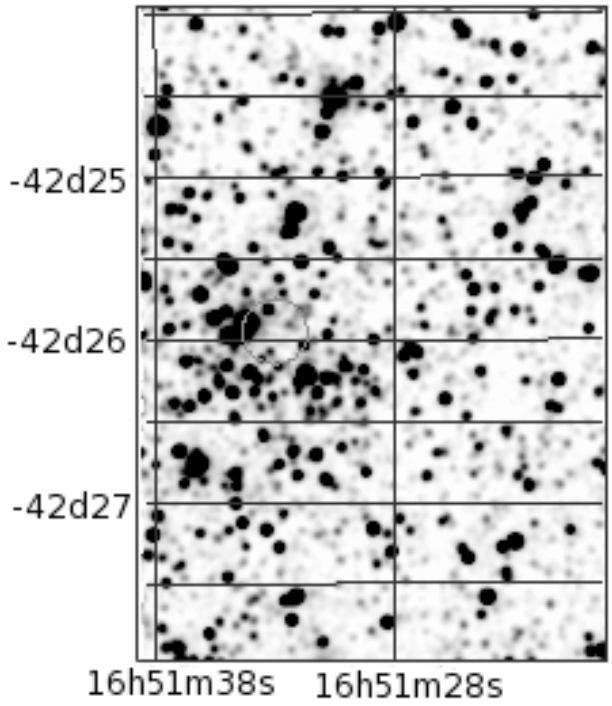

Fig. 3. 4′ × 4′ 2MASS H image of FSR 1744. Images provided by the 2MASS Image Service. The small circle indicates the optimized central coordinates (Cols. 5 and 6 of Table 1).

OC analysis (e.g. Bonatto & Bica 2007, and references therein) shows that as long as no other populous cluster is present in the field, and differential absorption is not prohibitive wide extraction areas can provide the required statistics, in terms of magnitude and colours, for a consistent field star decontamination (Sect. 4.2). They also produce more constrained stellar radial density profiles (Sect. 5). The extraction radii are 20′, 20′, and 50′, respectively for FSR 1744, FSR 89 and FSR 31. Such radii are ≈30 and ≈4 times larger than the respective core and limiting radii (Sect. 5).

As a photometric quality constraint, 2MASS extractions were restricted to stars with magnitudes *(i)* brighter than those of the 99.9% Point Source Catalogue completeness limit[4] in the cluster direction, and *(ii)* with errors in J, H and K_s smaller than 0.2 mag. The 99.9% completeness limits are different for each cluster, varying with Galactic coordinates.

To objectively characterize the distribution of 2MASS photometric uncertainties in the fields of the present objects, we show in Fig. 6 cumulative histograms with the fraction of stars as a function of uncertainties for the 3 bands. Projected areas sampled in the histograms correspond to the respective extraction radius of each object. The distributions of photometric uncertainties are similar both among the fields sampled and 2MASS bands. The fraction of stars with J, H and K_s uncertainties

[4] Following the Level 1 Requirement, according to `www.ipac.caltech.edu/2mass/releases/allsky/doc/sec6_5a1.html`

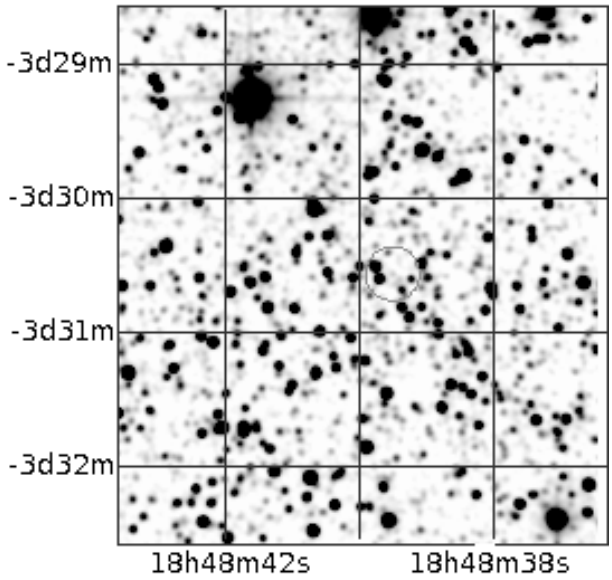

Fig. 4. Same as Fig. 3 for FSR 89.

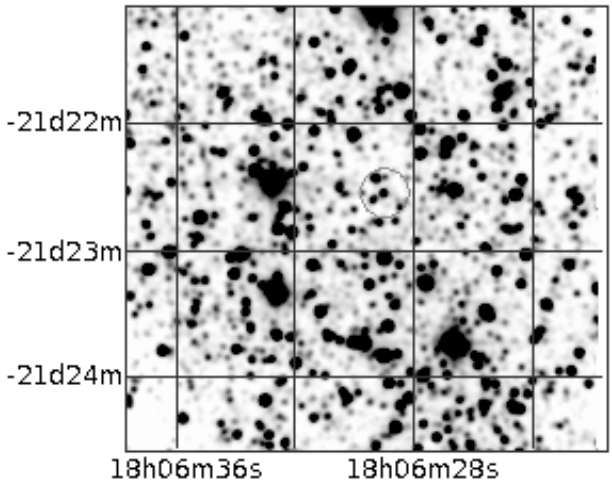

Fig. 5. Same as Fig. 3 for FSR 31.

smaller than 0.06 mag in FSR 1744, FSR 89 and FSR 31 ranges from ≈75–85%.

For reddening transformations we use the relations $A_J/A_V = 0.276$, $A_H/A_V = 0.176$, $A_{K_s}/A_V = 0.118$, and $A_J = 2.76 \times E(J-H)$ (Dutra et al. 2002), assuming a constant total-to-selective absorption ratio $R_V = 3.1$.

4.2. CMD morphology and field-star decontamination

4.2.1. FSR 1744

2MASS $J \times (J-H)$ and $J \times (J-K_s)$ CMDs extracted from a central ($R < 2'$) region of FSR 1744 are presented in Fig. 7. In this extraction that contains the bulk of the cluster stars (Sect. 5), a disk-like population ($0.2 \lesssim (J-H) \lesssim 0.8$ and $J \lesssim 15$) appears to merge into a redder component ($(J-H) \gtrsim 0.8$). With respect to the equal-area comparison field extraction, the red component clearly presents an excess in the number of stars for $1.1 \lesssim (J-H) \lesssim 1.5$ and $13.3 \lesssim J \lesssim 14.7$ (top-left panel), which resembles a giant clump of an intermediate-age OC. Similar features are present in the $J \times (J-K_s)$ CMD (top-right panel).

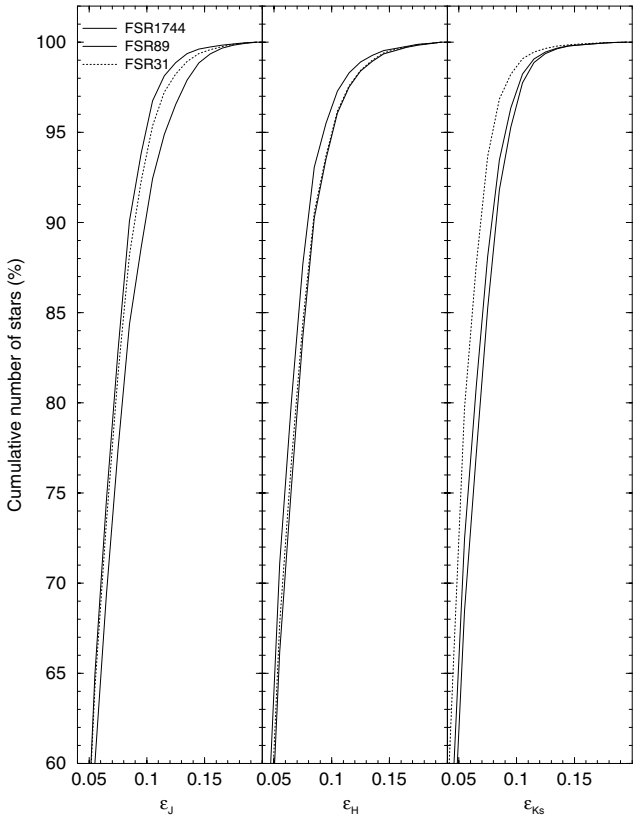

Fig. 6. 2MASS photometric errors evaluated by me cumulative histograms with the fraction of stars as a function of uncertainties. In all cases, a large fraction of the stars have uncertainties smaller than 0.06 mag.

To uncover the intrinsic CMD morphology we apply the field star decontamination algorithm described in Bonatto & Bica (2007). The algorithm works on a statistical basis that takes into account the relative number-densities of probable field and cluster stars in small cubic CMD cells. Cell axes correspond to the magnitude J and the colours $(J-H)$ and $(J-K_s)$ (considering as well the 1σ uncertainties in the 2MASS bands). These are the 2MASS colours that provide the maximum variance among CMD sequences for OCs of different ages (e.g. Bonatto et al. 2004).

The algorithm *(i)* divides the full range of magnitude and colours of a given CMD into a 3D grid, *(ii)* computes the expected number-density of field stars in each cell based on the number of comparison field stars with magnitude and colours compatible with those of the cell, and *(iii)* randomly subtracts the expected number of field stars from each cell. The algorithm is sensitive to local variations of field-star contamination with colour and magnitude (Bonatto & Bica 2007). Typical cell dimensions are $\Delta J = 0.5$, and $\Delta(J-H) = \Delta(J-K_s) = 0.2$. These values are large enough to allow sufficient star-count statistics in individual cells and small enough to preserve the morphology of different CMD evolutionary sequences. 2MASS photometric uncertainties for most stars of the present objects are considerably smaller than the adopted cell dimensions (Fig. 6). As the comparison field we use the region $6 < R(') < 20$ around the cluster center to obtain representative background star-count statistics.

To minimize potential artifacts introduced by the choice of parameters, the algorithm is applied for 3 different grid specifications in each dimension. For instance, for a CMD grid starting at magnitude J_0 (and cell width ΔJ), additional runs for $J_0 \pm \frac{1}{3}\Delta J$

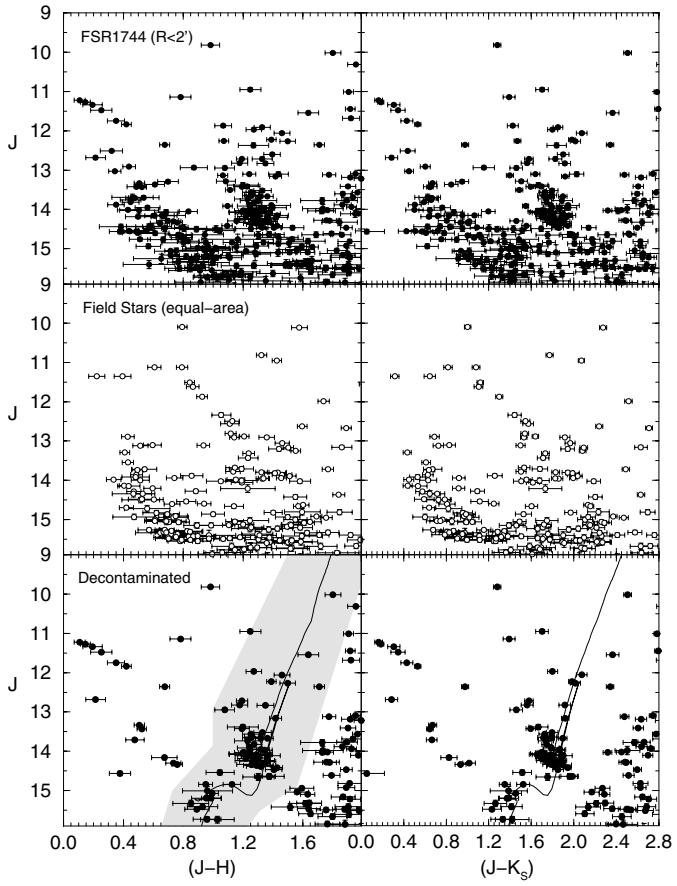

Fig. 7. 2MASS CMDs extracted from the $R < 2'$ region of FSR 1744. *Top panels*: observed photometry with the colours $J \times (J-H)$ (*left*) and $J \times (J-K_s)$ (*right*). *Middle*: equal-area comparison field. Besides contamination of disk and bulge stars, evidence of a giant clump shows up at $1.1 \lesssim (J-H) \lesssim 1.5$, $1.5 \lesssim (J-K_s) \lesssim 2.0$ and $13.3 \lesssim J \lesssim 14.7$. *Bottom panels*: field star decontaminated CMDs set with the 1 Gyr Padova isochrone (solid line), where the giant clump and the top fraction of the MS are conspicuous in both colours. The colour-magnitude filter used to isolate cluster MS/evolved stars is shown as a shaded region.

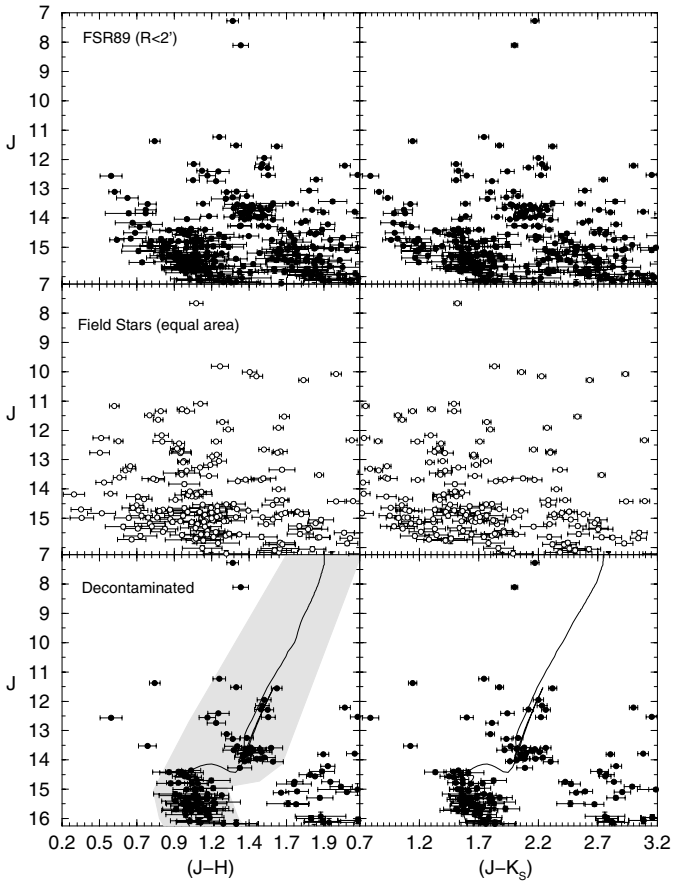

Fig. 8. Same as Fig. 7 for the $R < 2'$ region of FSR 89. In this case the giant clump and about 2 mag of the MS are present in both CMDs. The stellar sequences were fitted with the 1 Gyr Solar metallicity Padova isochrone.

are included. Considering as well the 2 colours, 27 different outputs are obtained, from which the average number of probable cluster stars $\langle N_{\rm cl} \rangle$ results. Typical standard deviations of $\langle N_{\rm cl} \rangle$ are at the ≈2.5% level. The final field star-decontaminated CMD contains the $\langle N_{\rm cl} \rangle$ stars with the highest number-frequencies. Stars that remain in the CMD after field star decontamination are in cells where the stellar density presents a clear excess over the field. Consequently, they have a significant probability of being cluster members. Further details on the algorithm, including discussions on subtraction efficiency and limitations, are given in Bonatto & Bica (2007).

The resulting field star decontaminated CMDs are shown in the bottom panels of Fig. 7. As expected, most of the disk component is removed, leaving two groups of stars that resemble the top of a main sequence (MS) and a giant clump. Residual contamination, mostly from bulge stars, occurs especially in the red domain. Essentially the same CMD features result in both colours.

Cluster fundamental parameters are derived with solar-metallicity Padova isochrones (Girardi et al. 2002) computed with the 2MASS J, H and K_s filters[5]. The 2MASS transmission filters produced isochrones very similar to the Johnson-Kron-Cousins (e.g. Bessel & Brett 1988) ones, with differences of at most 0.01 in $(J-H)$ (Bonatto et al. 2004). Considering uncertainties in the isochrone fit, we obtain an age of 1.0 ± 0.1 Gyr, reddening $E(J-H) = 0.80 \pm 0.03$, which converts to $E(B-V) = 2.56 \pm 0.12$, and $A_V = 7.9 \pm 0.4$ (Dutra et al. 2002). The distance of FSR 1744 from the Sun is $d_\odot = 3.5 \pm 0.1$ kpc. With the recently derived value of the Sun's distance to the Galactic center $R_\odot = 7.2$ kpc (Bica et al. 2006), we conclude that FSR 1744 is located at a Galactocentric distance $R_{\rm GC} = 4.0 \pm 0.1$ kpc.

[5] stev.oapd.inaf.it/~lgirardi/cgi-bin/cmd

4.2.2. FSR 89

CMDs in both colours of the $R < 2'$ region of FSR 89 are given in Fig. 8. They were analysed similarly to those of FSR 1744 (Sect. 4.2.1). For FSR 89 we take as comparison field the region $10 < R(') < 20$. Similarly to FSR 1744, the field star decontaminated CMDs (bottom panels) present a conspicuous giant clump and about 2 mag of the MS. They imply an age of 1.0 ± 0.1 Gyr, $E(J-H) = 0.92 \pm 0.03$ ($E(B-V) = 2.94 \pm 0.12$), and $A_V = 9.1 \pm 0.4$. Its distance from the Sun is $d_\odot = 2.2 \pm 0.1$ kpc, which puts it at $R_{\rm GC} = 5.4 \pm 0.1$ kpc.

4.2.3. FSR 31

Figure 9 shows the CMD analysis of the $R < 3'$ region of FSR 31. The comparison field corresponds to the region $10 < R(') < 50$. An interval of about 3 mag of the MS, and the RGB

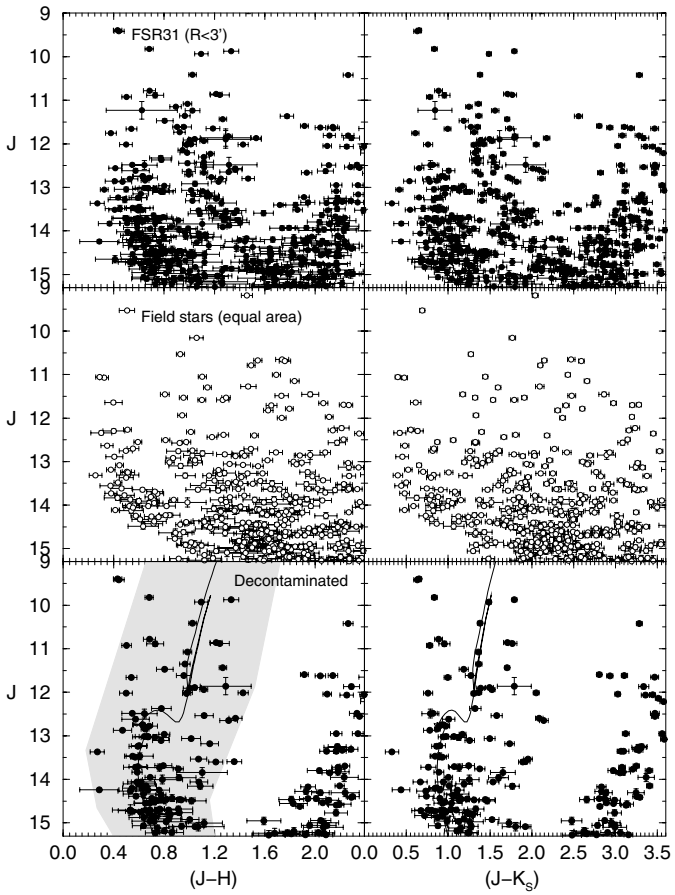

Fig. 9. Same as Fig. 7 for the $R < 3'$ region of FSR 31. In this case the RGB and about 3 mag of the MS are present in both CMDs. The stellar sequences were fitted with the 1.1 Gyr Solar metallicity Padova isochrone.

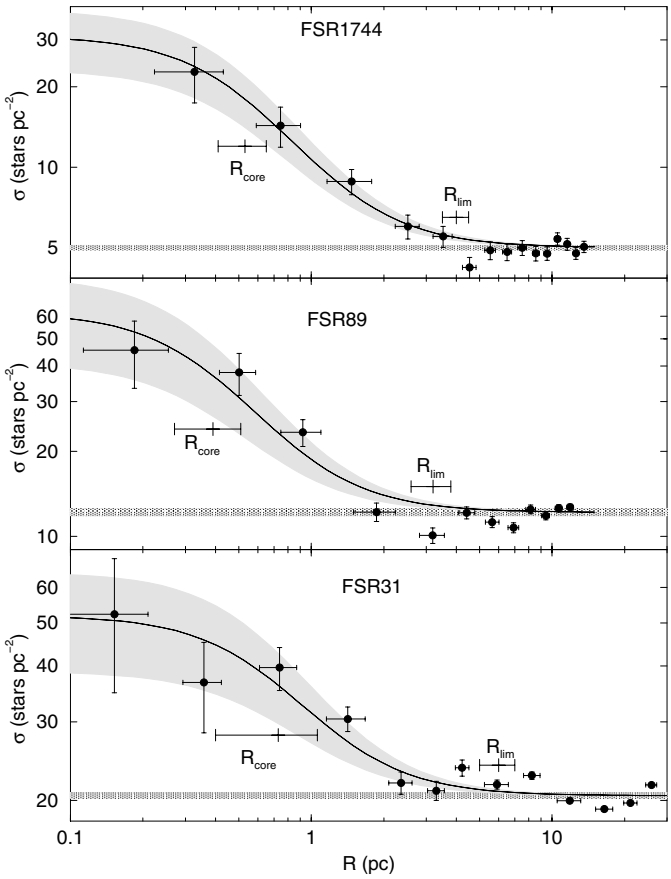

Fig. 10. Stellar RDPs (filled circles) given in absolute scale. Solid lines: best-fit King-like profile. Horizontal shaded region: stellar background level measured in the comparison field. Core and limiting radii are indicated. Gray regions: 1σ fit uncertainty.

sequence, are present in both CMDs (bottom panels). From them we derive an age of 1.1 ± 0.1 Gyr, $E(J-H) = 0.46 \pm 0.02$ ($E(B-V) = 1.47 \pm 0.07$), and $A_V = 4.6 \pm 0.2$. Its distance from the Sun is $d_\odot = 1.6 \pm 0.1$ kpc, which locates it at $R_{\rm GC} = 5.6 \pm 0.1$ kpc.

4.2.4. Cluster ages

It is interesting that the present three clusters have comparable ages of $\approx$1 Gyr. Rather than a coincidence, this fact probably reflects a selection effect, in the sense that if the clusters were significantly younger with more luminous stars, they would have already been identified in previous surveys. Our experience with age derivation of intermediate/old age OCs using Padova isochrones applied to field-star decontaminated CMDs shows that the solutions are usually rather constrained, with uncertainties smaller than 20% (Bonatto & Bica 2007). Conversely, this result might be providing clues to the time-scale for cluster dissolution at the their Galactocentric distance and respective masses.

5. Structural parameters

Cluster structure is investigated by means of the stellar radial density profile (RDP), built with colour–magnitude (CM) filtered photometry (Bonatto & Bica 2007, and references therein). CM filters are used to remove stars with colours compatible with those of the foreground/background field. They are wide enough to accommodate cluster MS and evolved star colour distributions, allowing for 1σ uncertainties. However, residual field stars with colours similar to those of the cluster are expected to remain in the CM filter. This residual contamination is statistically evaluated using the comparison field. CM filter widths should also account for formation or dynamical evolution-related effects, such as enhanced fractions of binaries (and other multiple systems) towards the central parts of clusters, since such systems tend to widen the MS (e.g. Bonatto & Bica 2007; Bonatto et al. 2005; Hurley & Tout 1998; Kerber et al. 2002).

To avoid oversampling near the centre and undersampling at large radii, RDPs are built by counting stars in rings of increasing width with distance to the centre. The number and width of rings are adjusted to produce RDPs with adequate spatial resolution and as small as possible 1σ Poisson errors. The residual background level of each RDP corresponds to the average number of CM-filtered stars measured in the comparison field. The R coordinate and respective uncertainty of each ring corresponds to the average position and standard deviation of the stars inside the ring.

The resulting profiles are given in Fig. 10. The RDPs are fitted with the analytical profile $\sigma(R) = \sigma_{\rm bg} + \sigma_{0\,\rm K}/(1+(R/R_{\rm core})^2)$, where $\sigma_{\rm bg}$ is the residual background density, $\sigma_{0\,\rm K}$ is the central density of stars, and $R_{\rm core}$ is the core radius. This function is similar to that introduced by King (1962) to describe the surface brightness profiles in the central parts of globular clusters. In all cases the adopted King-like function well describes the RDPs,

Table 2. Structural parameters from CM-filtered photometry

		RDP				
Cluster	1′	$\sigma_{\rm bg}$	$\sigma_{0\ \rm K}$	$\delta_{\rm c}$	$R_{\rm core}$	$R_{\rm lim}$
	(pc)	(stars pc^{-2})	(stars pc^{-2})		(pc)	(pc)
(1)	(2)	(3)	(4)	(5)	(6)	(7)
FSR 1744	1.002	5.0 ± 0.1	26 ± 8	5.2 ± 1.6	0.53 ± 0.12	4.0 ± 0.5
FSR 89	0.623	12.2 ± 0.2	50 ± 21	4.1 ± 1.7	0.39 ± 0.12	3.2 ± 0.6
FSR 31	0.466	20.5 ± 0.2	32 ± 13	1.5 ± 0.6	0.73 ± 0.33	6.0 ± 1.0

Column 2: arcmin to parsec scale. To minimize degrees of freedom in RDP fits with the King-like profile (see text), $\sigma_{\rm bg}$ was kept fixed (measured in the respective comparison fields) while $\sigma_{0\ \rm K}$ and $R_{\rm core}$ were allowed to vary, Col. 5: cluster/background density contrast ($\delta_{\rm c} = \sigma_{0\ \rm K}/\sigma_{\rm bg}$), measured in CM-filtered RDPs.

within uncertainties. $\sigma_{0\ \rm K}$ and the core radius ($R_{\rm core}$) are derived from the RDP fit, while $\sigma_{\rm bg}$ is measured in the respective comparison field. They are given in Table 2, and the best-fit solutions are superimposed on the CM-filtered RDPs (Fig. 10). Because of the 2MASS photometric limit, $\sigma_{0\ \rm K}$ corresponds to a cutoff for stars brighter than $J \approx 15.6$, ≈16 and ≈15.3, respectively for FSR 1744, FSR 89 and FSR 31.

Piskunov et al. (2007b) computed the core radii and tidal masses for a sample of 236 OCs distributed a few kpcs from the Sun. With the core radii derived in the present paper (Table 2), FSR 31, FSR 1744 and especially FSR 89 populate the small-core radius tail of the distribution given by Piskunov et al. (2007b).

The residual background contamination can be quantified by the density contrast parameter $\delta_{\rm c} = \sigma_{0\ \rm K}/\sigma_{\rm bg}$ (Col. 5 of Table 2). Because it is the most centrally projected OC of the present sample, FSR 31 presents the lowest $\delta_{\rm c}$, about 1/3 of the value of the other two OCs. Since $\delta_{\rm c}$ is measured in CM-filtered RDPs, it does not necessarily correspond to the visual contrast produced by observed stellar distributions in 2MASS images (Figs. 3–5).

We also provide in Col. 7 of Table 2 the cluster limiting radius and uncertainty, which are estimated by comparing the RDP (taking into account fluctuations) with the background level. $R_{\rm lim}$ corresponds to the distance from the cluster centre where RDP and background become statistically indistinguishable. For practical purposes, most of the cluster stars are contained within $R_{\rm lim}$. The limiting radius should not be mistaken for the tidal radius; the latter values are usually derived from King (or other analytical functions) fits to RDPs, which depend on wide surrounding fields and as small as possible Poisson errors (e.g. Bonatto & Bica 2007). In contrast, $R_{\rm lim}$ comes from a visual comparison of the RDP and background level.

The empirical determination of a cluster-limiting radius depends on the RDP and background levels (and respective fluctuations). Thus, dynamical evolution may indirectly affect the measurement of the limiting radius. Since mass segregation preferentially drives low-mass stars to the outer parts of clusters, the cluster/background contrast in these regions tends to lower as clusters age. As an observational consequence, smaller values of limiting radii should be measured, especially for clusters in dense fields. However, simulations of King-like OCs (Bonatto & Bica 2007) show that, provided not exceedingly high, background levels may produce limiting radii underestimated by about 10–20%. The core radius, on the other hand, is almost insensitive to background levels (Bonatto & Bica 2007). This occurs because $R_{\rm core}$ results from fitting the King-like profile to a distribution of RDP points, which minimizes background effects.

5.1. Cluster mass

Because of the distance from the Sun and the 2MASS photometric limits (Sect. 4.1), the MS mass range results too narrow to allow computation of the mass function (MF) for FSR 1744 and FSR 89. In those cases we simply computed the mass of the observed (background-subtracted) MS and evolved stars. The results are $M_{\rm obs} = 160 \pm 33\,M_{\odot}$ for FSR 1744 and $M_{\rm obs} = 143 \pm 20\,M_{\odot}$ for FSR 89. For FSR 31 the observed mass is $M_{\rm obs} = 483 \pm 55\,M_{\odot}$. The MF $\left(\phi(m) \propto m^{-(1+\chi)}\right)$ of FSR 31 could be computed, resulting in a slope $\chi = 1.8 \pm 0.9$. Extrapolation of the MF to the H-burning mass limit ($m = 0.08\,M_{\odot}$) assuming the universal Initial Mass Function of Kroupa (2001) produces a total mass of $M_{\rm total} = (5.1 \pm 2.3) \times 10^3\,M_{\odot}$. The latter value should be taken as an upper limit, since ∼1 Gyr of dynamical evolution may have driven a significant fraction of the low-mass content to the field (e.g. Bonatto & Bica 2007; Bonatto & Bica 2005). Low-mass stars spend most of their lives in the outer parts of clusters because their binding energies are smaller and thus have higher probability of escape (e.g. Aarseth 1971, 2005). Low-mass star depletion has been investigated in N-body simulations of star clusters in external tidal fields by e.g. Baumgardt & Makino (2003), who found that the depletion may be strong enough to change an initially increasing mass function into a decreasing one towards low-mass stars. The observed mass values of FSR 31, FSR 1744 and FSR 89 (∼140–480 $M_{\odot}$) are slightly lower than the average cluster mass of the tidal mass distribution given by Piskunov et al. (2007b).

6. Discussion

The preceding sections indicate that we are studying Gyr-class OCs located in the inner Galaxy. Clusters in that region are subject to important tidal interactions in the form of shocks due to disk and bulge crossings, as well as encounters with massive molecular clouds. Over large time periods, these processes tend to dynamically heat a star cluster, which enhances the rate of low-mass star evaporation and produces an increase of the cluster in all scales. For some clusters, on the other hand, mass segregation and evaporation may also lead to a phase of core contraction (Sect. 2). Consequently, these effects tend to disrupt most clusters, especially the less populous ones.

To put FSR 1744, FSR 89 and FSR 31 into perspective we compare in Fig. 11 their properties with those of a sample of *(i)* bright nearby OCs (Bonatto & Bica 2005); *(ii)* young OCs (Bonatto et al. 2006b,c); and *(iii)* OCs projected against the central parts of the Galaxy (Bonatto & Bica 2007). OCs in sample *(i)* have ages in the range $70 \lesssim \mathrm{age(Myr)} \lesssim 7000$, masses within $400 \lesssim M(M_{\odot}) \lesssim 5300$, and Galactocentric distances in the range

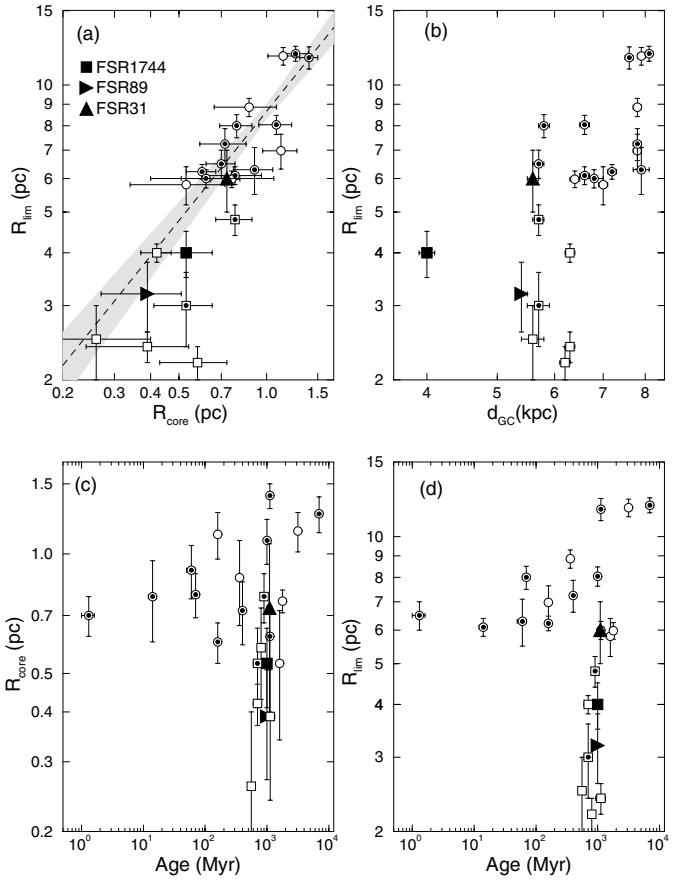

Fig. 11. Relations involving structural parameters of OCs. Circles: nearby OCs, including two young ones. Squares: OCs projected on dense fields towards the centre. Symbols with dots: OCs more massive than 1000 $M_{\odot}$.

$5.8 \lesssim R_{\rm GC}(\rm kpc) \lesssim 8.1$. The OCs in sample *(ii)* are NGC 6611 with age ≈1.3 Myr, $M = 1600\,M_{\odot}$ and $R_{\rm GC} = 5.5$ kpc, and NGC 4755 with age ≈14 Myr, $M = 1150\,M_{\odot}$ and $R_{\rm GC} = 6.4$ kpc. Sample *(iii)* OCs are characterized by $600 \lesssim$ age(Myr) $\lesssim 1300$, $210 \lesssim M(M_{\odot}) \lesssim 3100$, and $5.6 \lesssim R_{\rm GC}(\rm kpc) \lesssim 6.3$.

Core and limiting radii of the OCs in samples *(i)* and *(ii)* are almost linearly related by $R_{\rm lim} = (8.9\pm0.3)\times R_{\rm core}^{(1.0\pm0.1)}$ (panel (a)), which suggests that both kinds of radii undergo a similar scaling, in the sense that on average, larger clusters tend to have larger cores, at least for $0.5 \lesssim R_{\rm core}(\rm pc) \lesssim 1.5$ and $5 \lesssim R_{\rm lim}(\rm pc) \lesssim 15$. Linear relations between the core and limiting radii in OC samples were also found by Nilakshi et al. (2002), Sharma et al. (2006), and Maciejewski & Niedzielski (2007). However, two-thirds of the OCs in sample *(iii)* do not follow that relation, which suggests that they are either intrinsically small or have suffered important evaporation effects (Sect. 2). The core and limiting radii of FSR 1744, FSR 89 and FSR 31 are consistent with the relation at the 1σ level.

A dependence of open cluster size on Galactocentric distance is implied by panel (b), as previously suggested by Lyngå (1982) and Tadross et al. (2002). In this context, the limiting radii of FSR 1744, FSR 89 and FSR 31 are consistent with their positions in the Galaxy. Considering the linear relation between core and limiting radii (panel a), a similar conclusion applies to the core radius. Part of this relation may be related to a primordial effect, in the sense that the higher density of molecular gas in the central Galactic regions may have produced clusters with smaller core radii, as suggested by van den Bergh et al. (1991) to explain the increase of globular cluster radii with Galactocentric distance.

In panels (c) and (d) we compare core and limiting radii with cluster age, respectively. This relationship is intimately related to cluster survival/dissociation rates. Both kinds of radii present a similar dependence on age, in which part of the clusters – especially those more massive than $1000\,M_{\odot}$– expand with time, while some seem to shrink. The bifurcation occurs at age ∼1 Gyr. FSR 1744 and FSR 89, the innermost OCs of the present work, have core and limiting radii typical of the small OCs in the lower branch.

A similar effect was observed for the core radii of LMC and SMC star clusters (Wilkinson et al. 2003; Mackey & Gilmore 2003). These clusters have core radii ($0.5 \lesssim R_{\rm core}(\rm pc) \lesssim 8$) and mass ($10^3 \lesssim M(M_{\odot}) \lesssim 10^6$) significantly larger than the present ones. The core radii distribution of most LMC and SMC clusters is characterized by a trend of increasing $R_{\rm core}$ with age with an apparent bifurcation (core shrinkage) at several hundred Myr. Mackey & Gilmore (2003) argue that this relationship represents true physical evolution, with some clusters developing expanded cores due to an as yet unidentified physical process.

At least two effects may combine to produce the smaller core radius distribution presented by the Galactic OCs compared to the LMC/SMC ones. The shorter core collapse time-scale associated with lower mass clusters makes core collapse by dynamical friction a very plausible explanation. At the same time, probably because of their significantly lower masses, Galactic OCs seem to suffer more severe tidally-induced shrinkage effects than LMC/SMC clusters.

Besides dynamic interactions, star clusters projected against the central parts of the Galaxy – especially the poorly-populated ones – may suffer from low-contrast effects. Such clusters are expected to be the majority in the Galaxy (e.g. Bonatto et al. 2006a). When centrally projected, the limiting radii of poorly-populated OCs may be underestimated by about 10–20%; the core radii, on the other hand, are not affected (Bonatto & Bica 2007). In this sense, the small sizes of FSR 1744 and FSR 89 (and to a lesser extent FSR 31), especially the core radii, appear to be related to dynamical effects.

Irrespective of age, inner OCs and central massive clusters are rarely detected. This is further made clear in Fig. 12 where the WEBDA OCs younger than 0.4 Gyr are plotted. On the other hand, more than 102 embedded clusters and candidates with $|l| < 30^{\circ}$ are catalogued. Before the year 2003, 34 such objects were catalogued by Bica et al. (2003b). In that same year, 68 new objects were found (Bica et al. 2003a; Dutra et al. 2003b) in the direction of nebulae. If the number of surviving open clusters in each generation corresponds to a fraction of ∼4% of the embedded ones (Lada & Lada 2003), it should be expected that about 1000 OCs per Gyr would survive the infant mortality phase. However, the number of OCs of any age in the inner Galaxy is very small (Figs. 1 and 12). This brings the recurrent question of whether inner Galaxy clusters cannot be observed because of strong absorption and crowding, or have been systematically dissolved by the different tidal effects (Sect. 1).

A more comprehensive picture of the cluster age and Galactocentric distance dependence is provided by the OC age distribution function $\phi(\tau) = \frac{{\rm d}N_{\rm OC}}{{\rm d}\tau}$. Before dealing with $\phi(\tau)$ we must consider how completeness affects the WEBDA sample. This issue has been investigated by Bonatto et al. (2006a) by means of simulations involving the actual 2MASS stellar background in the Galaxy. The main results are: *(i)* the completeness-corrected radial distribution of OCs follows the expected exponential-decay (disk) profile; *(ii)* OCs located at

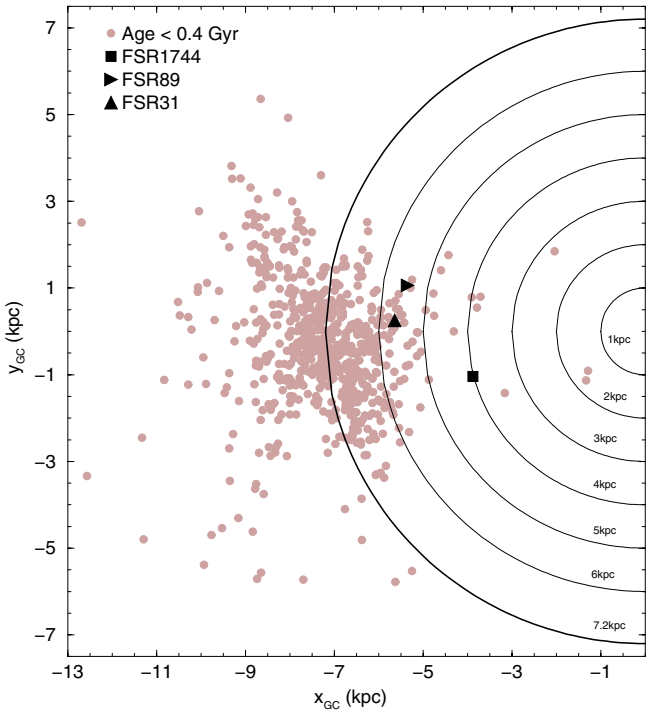

Fig. 12. Same as Fig. 1 for the WEBDA OCs with ages <0.4 Gyr (gray circles). The present Gyr-class OCs are also shown.

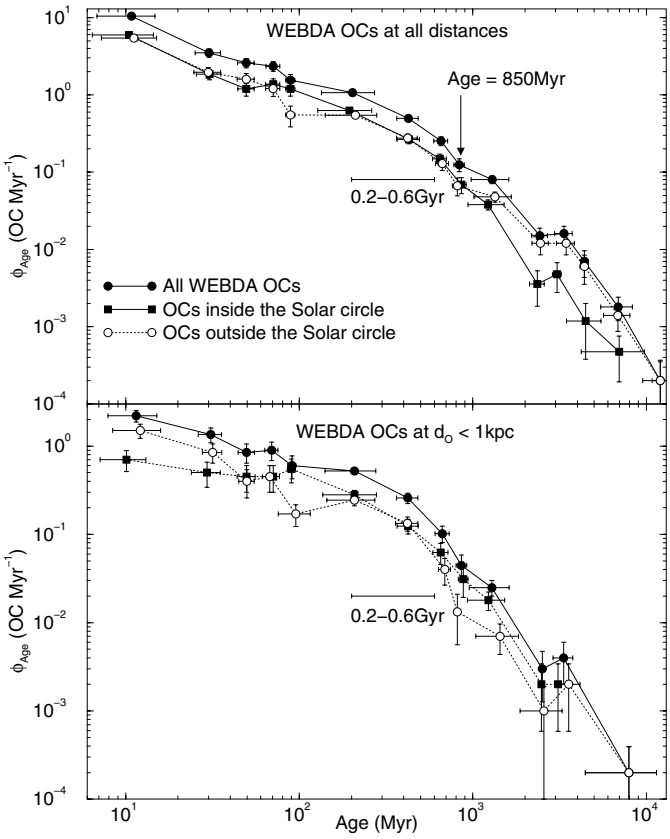

Fig. 13. *Top panel*: age distribution function for the WEBDA OCs, including FSR 1744, FSR 89 and FSR 31, located inside (filled squares) and outside (empty circles) the Solar circle, compared to the combined total WEBDA sample + FSR distribution (filled circles). The inside distribution has been normalized to the same number of OCs as outside the Solar circle. The difference in the OC number-density between both regions increases for ages >850 Myr. The excess in the OC number density at age ~200–600 Myr is indicated. Bottom panel: same as above for a selection of OCs with distance from the Sun <1 kpc.

$d_\odot \lesssim 1.3$ kpc are not much affected by completeness; *(iii)* as expected, completeness is more critical for OCs inside the Solar circle; *(iv)* disruption effects appear to become observationally relevant for OCs with $d_\odot \gtrsim 1.4$ kpc towards the Galactic center; and *(v)* OCs younger than 1 Gyr are more affected by completeness than older ones. The latter occurs because young OCs are found preferentially at lower Galactic latitudes (thus, high field-star density) than the old ones (Bonatto et al. 2006a). Obviously, very young OCs are easier to observe even in low-disk directions because of the presence of luminous stars.

As of May 2007, WEBDA contains 441 OCs with known age and distance located inside the Solar circle and 531 OCs outside it. With the inclusion also of FSR 1744, FSR 89 and FSR 31, the present sample represents an increase of ≈50% with respect to that used in Bonatto et al. (2006a). In Fig. 13 (top panel) we show the age-distribution functions for the full sample and for the OCs inside and outside the Solar circle. All the OCs contained in the age-distribution functions have survived the infant mortality phase (Sect. 2). For a better comparison, the age-distribution function of OCs inside the Solar circle has been normalized to the number of OCs outside the Solar circle (531). The main feature of both age-distributions is that they fall off with increasing slope with cluster age. Both are similarly flat, at 1 σ, for ages $\lesssim$850 Myr, which is consistent with the fact that most of these OCs are not old enough to have suffered significant disruption effects. Indeed, this age threshold is similar to the upper limit for the disruption time-scale of OCs less massive than 5000 $M_\odot$, $t_{\rm dis} \lesssim 900$ Myr (e.g. Lamers et al. 2005). For older ages, on the other hand, the number-density of OCs inside the Solar circle systematically falls off with age significantly faster than outside the Solar circle. According to the items *(iii)* to *(v)* above, the difference in the number-density of old OCs may be partly accounted for by completeness and partly by disruption, since ≈42% of the OCs inside the Solar circle are more distant than $d_\odot = 1.4$ kpc from the Sun. In addition, contrary to outside the Solar circle, the inner Galaxy appears not to host OCs older than ≈7 Gyr. These arguments are consistent with a Galactocentric-distance dependent OC disruption time-scale, coupled to decreasing completeness towards the central parts.

To minimize completeness and disruption effects, we also show in Fig. 13 (bottom panel) the age-distribution functions restricted to the OCs with distance from the Sun $d_\odot < 1$ kpc. The restricted age-functions contain 187 OCs inside the Solar circle and 173 outside. Within uncertainties, the distributions for OCs older than ~50 Myr are similar, except for the lack of OCs older than ≈7 Gyr inside the Solar circle. Another difference is the low frequency of OCs younger than ~50 Myr inside the Solar circle.

Qualitatively, the age-distribution functions for the WEBDA + present FSR sample (top panel) and especially for the $d_\odot <$ 1 kpc sample (bottom panel) are similar to that of a restricted region, $d_\odot < 600$ pc (Lamers et al. 2005), including the excess on the OC number density for ages in the range ~200–600 Myr. The shape of the age-distribution function of the OCs in this restricted region was shown to be consistent with the combined effects of the tidal field strength, GMC density and the dependence of disruption on cluster mass (Lamers & Gieles 2006).

Automated infrared surveys such as that of Froebrich et al. (2007b) could provide observational clues to settle the tidal dissolution *vs* completeness issue. Based on over-density

arguments, they found 89 candidates within $|l| < 30°$. However, they concluded that ≈50% of their objects are possibly field fluctuations. Studies like Kharchenko's (2005) that use proper-motion data to determine cluster members, or the approach that we use which is based on CMD and radial density profile decontamination can assess an open cluster nature. Among the 89 Froebrich et al. (2007b) candidates towards the central parts, FSR 1744, FSR 89 and FSR 31 are the best cases. A preliminary conclusion based on image inspection is that we do not expect to find a significantly larger number of OCs in the Froebrich et al. (2007b) central sample. More studies like the present one providing decontaminated CMDs and profile information are necessary to better determine the fraction of actual clusters.

7. Concluding remarks

Fundamental and structural parameters of the open clusters FSR 1744, FSR 89 and FSR 31 were derived in the present work. These objects are included in the catalogue of candidate star clusters of Froebrich et al. (2007b), which is an automated survey for overdensities in the near-infrared. The present results are based on field-star decontaminated 2MASS CMDs and stellar density profiles, using analysis algorithms from Bonatto & Bica (2007), and references therein. They are confirmed to be Gyr-class open clusters located in the inner Galaxy, at R_{GC} = 4.0–5.6 kpc, with absorptions in the range A_V = 4.6–9.1 mag. Compared to nearby open clusters, they show small core and limiting radii, which appears to be related to a ∼Gyr-long period of tidal interactions with the bulge, disk and possibly molecular clouds. They are apparently dynamical survivors in a region where most open clusters are short-lived. In fact, the age-distribution of open clusters inside the Solar circle presents a deficiency of clusters older than ≈850 Myr with respect to the outer age-distribution.

A preliminary inspection of the candidates in Froebrich et al. (2007b) for $|l| < 30°$ suggests that the number of unknown star clusters must not be large, since they expect an important fraction of their targets to be field fluctuations. However, to establish their nature the candidates should be explored in more detail with field-decontamination filters such as proper motion, CMD and stellar density profiles. Besides a natural improvement on the statistics of the open cluster parameter space, another important result would be a better definition of the open cluster age-distribution function, especially in the inner Galaxy. The present work represents a step in that direction.

Acknowledgements. We thank the anonymous referee for comments and suggestions. We acknowledge partial financial support from the Brazilian agency CNPq.

References

Aarseth, S.J. 1971, Astrophys. Space Sci., 14, 188
Bastian, N., & Goodwin, S. P. 2006, MNRAS, 369, L9
Baumgardt, H., & Makino, J. 2003, MNRAS, 340, 227
van den Bergh, S. 1957, ApJ, 125, 445
van den Bergh, S., & McLure, R. D. 1980, A&A, 88, 360
van den Bergh, S., Morbey, C., & Pazder, J. 1991, ApJ, 375, 594
Bergond, G., Leon, S., & Guilbert, J. 2001, A&A, 377, 462
Bessel, M. S., & Brett, J. M. 1988, PASP, 100, 1134
Bica, E., Dutra, C. M., Soares, J., & Barbuy, B. 2003a, A&A, 404, 223
Bica, E., Dutra, C. M., & Barbuy, B. 2003b, A&A, 397, 177
Bica, E., Bonatto, C., Barbuy, B., & Ortolani, S. 2006, A&A, 450, 105
Boily, C., & Kroupa, P. 2002, in Modes of Star Formation and the Origin of Field Populations, ed. E. Grebel & W. Brandner, ASP Conf. Ser., 285, 141
Bonatto, C., & Bica, E. 2005, A&A, 437, 483
Bonatto, C., & Bica, E. 2007, MNRAS, 377, 1301
Bonatto, C., Bica, E., & Girardi, L. 2004, A&A, 415, 571
Bonatto, C., Bica, E., & Santos Jr., J. F. C. 2005, A&A, 433, 917
Bonatto, C., Kerber, L. O., Bica, E., & Santiago, B. X. 2006a, A&A, 446, 121
Bonatto, C., Santos Jr., J. F. C., & Bica, E. 2006b, A&A, 445, 567
Bonatto, C., Bica, E., Ortolani, S., & Barbuy, B. 2006c, A&A, 453, 121
Clark, J. S., Negueruela, I., Crowther, P. A., & Goodwin, S.P. 2005, A&A, 434, 949
Crowther, P. A., Hadfield, L. J., Clark, J. S., Negueruela, I., & Vacca, W. D. 2006, MNRAS, 372, 1407
Djorgovski, S., & Meylan, G. 1994, AJ, 108, 1292
Dutra, C. M., Santiago, B. X., & Bica, E. 2002, A&A, 383, 219
Dutra, C. M., Ortolani, S., Bica, E., Barbuy, B., Zoccali, M., & Momany, Y. 2003a, A&A, 408, 127
Dutra, C. M., Bica, E., Soares, J., & Barbuy, B. 2003b, A&A, 400, 533
Eisenhauer, F., Genzel, R., Alexander, T. et al. 2005, ApJ, 628, 246
Elson, R. A. W., & Fall, S. M. 1985, ApJ, 299, 211
Figer, D. F., Kim, S. S., Morris, M., et al. 1999, ApJ, 525, 750
Figer, D. F., Najarro, F., Gilmore, D., et al. 2002, ApJ, 581, 258
Figer, D. F., MacKenty, J. W., Robberto, M., et al. 2006, ApJ, 643, 1166
Friel, E. D. 1995, ARA&A, 33, 381
Froebrich, D., Meusinger, H., & Scholz, A. 2007a, MNRAS, 377, L54
Froebrich, D., Scholz, A., & Raftery, C. L. 2007b, MNRAS, 374, 399
de La Fuente Marcos, R. 1997, A&A, 322, 764
de La Fuente Marcos, R. 1998, A&A, 333, L27
de la Fuente Marcos, R., & de la Fuente Marcos, C. 2002, Ap&SS, 280, 381
Gieles, M., Portegies Zwart, S. F., Baumgardt, H., et al. 2006, MNRAS, 371, 793
Girardi, L., Bertelli, G., Bressan, A., et al. 2002, A&A, 391, 195
Goodwin, S. P., & Bastian, N. 2006, MNRAS, 373, 752
Hodge, P. 1987, PASP, 99, 724
von Hoerner, S. 1958, ApJ, 44, 221
Hurley, J., & Tout, A. A. 1998, MNRAS, 300, 977
Janes, K., & Adler, D. 1982, ApJ, 49, 425
Kerber, L. O., Santiago, B. X., Castro, R., & Valls-Gabaud, D. 2002, A&A, 390, 121
Khalisi, E., Amaro-Seoane, P., & Spurzem, R. 2007, MNRAS, 374, 703
Kharchenko, N. V., Piskunov, A. E., Röser, S., Schilbach, E., & Scholz, R.-D. 2005, A&A, 438, 1163
King, I. 1962, AJ, 67, 471
Kroupa, P. 2001, MNRAS, 322, 231
Kroupa, P., Aarseth, S., & Hurley, J. 2001, MNRAS, 321, 699
Lada, C. J., & Lada, E. A. 2003, ARA&A, 41, 57
Lamers, H. J. G. L. M., & Gieles, M. 2006, A&A, 455, L17
Lamers, H. J. G. L. M., Gieles, M., Bastian, N., et al. 2005, A&A, 441, 117
Lyngå, G. 1982, A&A, 109, 213
Maciejewski, G., & Niedzielski, A. 2007, A&A, 467, 1065
Mackey, A. D., & Gilmore, G. F. 2003, MNRAS, 338, 120
Mermilliod, J. C. 1996, in The Origins, Evolution, and Destinies of Binary Stars in Clusters, ed. E.F. Milone & J.-C. Mermilliod, ASP Conf. Ser., 90, 475
Nilakshi, S. R., Pandey, A. K., & Mohan, V. 2002, A&A, 383, 153
Nishiyama, S., Nagata, T., Sato, S., et al. 2006, ApJ, 647, 1093
Oort, J. H. 1958, in Ricerche Astronomische, 5, 63, Proc. of a Conference at Vatican Observatory, ed. D. J. K. O'Connell
Pavani, D. N., & Bica, E. 2007, MNRAS, 468, 139
Piskunov, A. E., Kharchenko, N. V., Röser, S., Schilbach, E., & Scholz, R.-D. 2007a, A&A, 445, 545
Piskunov, A. E., Schilbach, E., Kharchenko, N. V., Röser, S., & Scholz, R.-D. 2007b, A&A, 468, 151
Portegies Zwart, S. F., Makino, J., McMillan, S. L. W., & Hut, P. 2002, ApJ, 565, 265
Reid, N. 1993, ARA&A, 31, 345
Salaris, M., Weiss, A., & Percival, S. M. 2004, A&A, 422, 217
Sharma, S., Pandey, A. K., Ogura, K., et al. 2006, AJ, 132, 1669
Spitzer, L. 1958, ApJ, 127, 17
Tadross, A. L., Werner, P., Osman, A., & Marie, M. 2002, NewAst, 7, 553
Terlevich, E. 1987, MNRAS, 224, 193
Upgren, A. R., Mesrobian, W. S., & Kerridge, S. J. 1972, AJ, 77, 74
Wielen, R. 1991, in The Formation and Evolution of Star Clusters, ed. K. Janes, ASP Conf. Ser., 13, 343 (San Francisco, CA)
Wielen, R. 1971, A&A, 13, 309
Wielen, R. 1985, in Dynamics of Star Clusters, Proc. Symp. (Princeton, NJ. Dordrecht: Reidl), 449
Wilkinson, M. I., Hurley, J. R., Mackey, A. D., Gilmore, G. F. & Tout, C. A. 2003, MNRAS, 343, 1025